2-5-2003

Seasonal and Diurnal Variation of Geomagnetic Activity: Revised *Dst* Versus External Drivers

L V.T Hakkinen

T I. Pulkkinen

R J. Pirjola

H Nevanlinna

E I. Tanskanen

See next page for additional authors

Seasonal and diurnal variation of geomagnetic activity: Revised *Dst* versus external drivers

Lasse V. T. Häkkinen, Tuija I. Pulkkinen, Risto J. Pirjola, Heikki Nevanlinna, Eija I. Tanskanen, and Niescja E. Turner

Geophysical Research, Finnish Meteorological Institute, Helsinki, Finland

Received 3 April 2002; revised 16 September 2002; accepted 16 October 2002; published 5 February 2003.

[1] Daily and seasonal variability of long time series of magnetometer data from *Dst* stations is examined. Each station separately shows a local minimum of horizontal magnetic component near 18 local time (LT) and weakest activity near 06 LT. The stations were found to have different baselines such that the average levels of activity differed by about 10 nT. This effect was corrected for by introducing a new "base method" for the elimination of the secular variation. This changed the seasonal variability of the *Dst* index by about 3 nT. The hemispheric differences between the annual variation (larger activity during local winter and autumn solstice) were demonstrated and eliminated from the *Dst* index by addition of two Southern Hemisphere stations to a new index termed Dst_6. Three external drivers of geomagnetic activity were considered: the heliographic latitude, the equinoctial effect, and the Russell–McPherron effect. Using the newly created Dst_6 index, it is demonstrated that these three effects account for only about 50% of the daily and seasonal variability of the index. It is not clear what drives the other 50% of the daily and seasonal variability, but it is suggested that the station distribution may play a role. *INDEX TERMS:* 2784 Magnetospheric Physics: Solar wind/magnetosphere interactions; 2778 Magnetospheric Physics: Ring current; 2788 Magnetospheric Physics: Storms and substorms; 1555 Geomagnetism and Paleomagnetism: Time variations—diurnal to secular; *KEYWORDS: Dst* index, ring current, geomagnetic activity

Citation: Häkkinen, L. V. T., T. I. Pulkkinen, R. J. Pirjola, H. Nevanlinna, E. I. Tanskanen, and N. E. Turner, Seasonal and diurnal variation of geomagnetic activity: Revised *Dst* versus external drivers, *J. Geophys. Res.*, *108*(A2), 1060, doi:10.1029/2002JA009428, 2003.

1. Introduction

[2] Several studies have established that geomagnetic activity has a seasonal variability such that geomagnetic storms are both more intense and more numerous during equinoxes than during solstices [*Currie*, 1966; *Russell and McPherron,* 1973; *Clua de Gonzalez et al.*, 2001]. Furthermore, there is a diurnal variation in universal time (UT) convolved in this pattern; the *Dst* intensity is higher during the early morning and evening hours, and lower near 12 UT.

[3] Traditionally, these variations have been attributed to three external effects: Changes in the heliographic latitude of the Earth during the year [*Cortie*, 1912]; variations of the solar wind flow direction with respect to the Earth's magnetic dipole axis [*Bartels*, 1925; *McIntosh*, 1959]; and variation of the angle between the geocentric solar magnetospheric (GSM) equatorial plane and the solar equatorial plane [*Russell and McPherron*, 1973]. The Earth reaches extreme heliographic latitudes near equinoxes which leads to enhanced geomagnetic activity during those periods, as the Earth is then better connected to the fast solar wind streams from the low-latitude coronal holes. Decrease of the acute angle between the solar wind flow and the dipole axis during solstices seems to lead to a decrease in magnetic activity. This effect has been associated with geomagnetic activity being initiated by the onset of a Kelvin–Helmholtz instability at the dayside magnetopause, which is most likely to occur during equinoxes when the Earth's dipole axis is perpendicular to the solar wind flow [*Boller and Stolov*, 1970]. Reconnection at the subsolar magnetopause, and consequently geomagnetic activity, is enhanced if the magnetospheric field at the magnetopause, which is roughly along the GSM *Z* axis, is antiparallel with the interplanetary magnetic field (IMF). As the IMF is predominantly in the solar equatorial plane, such a situation occurs most often near equinoxes, when the Earth's rotation axis is oriented perpendicular to the Sun–Earth line, and the GSM *Z* axis has a smaller angle with respect to the solar equatorial plane. Studies evaluating the relative importance of these effects [e.g., *Cliver et al.*, 2000] are based on long-term averages of data and on careful inspection and interpretation of the relative minima and maxima that appear when the level of activity is displayed as a function of UT and day of year (DOY).

[4] Geomagnetic indices are based on magnetic records from observatory-quality magnetic stations. Those observatories that have operated over long time periods are especially important, as they provide long contiguous time

0148-0227/03/2002JA009428

series with accurately known baselines. Magnetic observatories today provide measurements of the three components of the full magnetic field vector in a digital form with an absolute accuracy of the order of a few nT; earlier they often provided the magnetic field recordings on photographic paper from where the values were digitized later. Therefore, the indices that are still widely used today were created in many ways as a compromise of what was available and of what was feasible in terms of manpower [*Mayaud*, 1980; *Menvielle and Berthelier*, 1991]. While these records are immensely useful in examination of long-term variability in the geomagnetic activity and solar–terrestrial coupling [e.g., *Vennerstrom and Friis-Christensen*, 1996; *Pulkkinen et al.*, 2001], they must be interpreted with care and understanding of their inherent limitations.

[5] The *Dst* index is created from measurements of the horizontal component of the magnetic field at four middle-latitude to low-latitude stations, and represents a measure of the intensity of geomagnetic storms [e.g., *Rangarajan*, 1989]. Traditionally, the *Dst* index has been interpreted to reflect variations in the intensity of the ring current encircling the Earth at distances ranging from 3 to 8 R_E. However, both early and more recent studies have shown that the *Dst* index also responds to other current systems in the magnetosphere: magnetopause currents [e.g., *Burton et al.*, 1975], tail currents [*Turner et al.*, 2000; *Alexeev et al.*, 1996], and currents induced in the Earth [*Häkkinen et al.*, 2002]. Thus, at times when the ring current is highly asymmetric [*Jordanova et al.*, 1998], interpretation of *Dst* variations in terms of changes in the magnetospheric current systems is not a straightforward process.

[6] In this paper we return to the topic of systematic seasonal and diurnal variations of the *Dst* index. We discuss the definition of *Dst* by considering the processing of magnetic data at individual stations and the selection of the stations used to create the *Dst* index. We examine what portion of the observed variability of *Dst* arises from the three effects mentioned above and what are their relative contributions.

[7] It is important to notice that while the *Dst* index is mainly used for analysis of magnetic storms, those periods cover only a minor portion of the time. Therefore, even if magnetic storms cause a majority of the negative excursions of the index, there may be other variations that have smaller intensity but dominate in occurrence frequency, and which then may also have their fingerprints in the diurnal and seasonal variability. Especially, even though it is clear that strong geomagnetic activity is driven by the solar wind and IMF, it is not necessarily clear that the entire data set dominated by quiet periods will show similar strong dependence on the driver properties. For these reasons, in this paper we will pay special attention also to the smaller effects such as baseline determinations and effects of the locations of the measuring stations.

[8] The method of computing the *Dst* index is discussed in detail in section 2. Especially we concentrate on the method of computing the disturbance fields at individual stations by removing the long-term secular variation and the daily *Sq* variation from the data.

[9] Section 3 is devoted to a thorough discussion about systematic differences in geomagnetic activity in the Northern and Southern Hemispheres. To minimize the influence of the hemispheric differences on the *Dst* index, we introduce a new index, Dst_6, which is based on data from three Northern Hemisphere and three Southern Hemisphere stations having as closely a symmetric longitude distribution as possible. In section 4, we evaluate the contributions of the three external effects to the seasonal and diurnal variations of Dst_6. Special attention is paid to the winter/summer and spring/fall asymmetries. We conclude that the three effects do not fully explain the variability of Dst_6 and that the relative significance of each effect is different for storm and nonstorm periods.

2. Computation of the *Dst* Index From Individual Station Data

2.1. Method of Computing the Official *Dst* Index

[10] *Dst* is an hourly index published since 1957 [*Sugiura and Kamei*, 1991]. It is computed from horizontal magnetic field variations recorded at four stations, Kakioka (KAK), Hermanus (HER), Honolulu (HON), and San Juan (SJG)

$$Dst(T) = \frac{1}{4}\sum_{i=1}^{4}\frac{\Delta H_i}{\cos\theta_i} \tag{1}$$

where ΔH_i are the variations of the horizontal magnetic field component (secular and *Sq* variations subtracted) at the four stations, and θ_i are the geomagnetic latitudes of the stations. Assuming that the disturbance is caused by a symmetric ring current encircling the Earth at the geomagnetic equator, that the Earth is small in comparison with the radius of the ring current and that there are no effects from induced currents, then terms $\Delta H_i/\cos\theta_i$ give the horizontal field variation at the geomagnetic equator. Thus, as the intensity of the recorded horizontal field variation depends on the station location, dividing by $\cos\theta$ gives a quantity that is a proxy for the intensity of the field caused by the external current system at the equator, independent of the station latitude. Therefore, in this analysis, we compute the quantities $\Delta H/\cos\theta$ for each station and compare those with each other. Figure 1 shows the locations of the *Dst* stations and of several other magnetic observatories and Table 1 gives their geographic and geomagnetic coordinates as well as data coverage used in this study.

[11] Note that *Sugiura and Kamei* [1991] give a somewhat different definition of the *Dst*, in which the horizontal disturbances are averaged separately, and the average is divided by the average of the cosines of the latitudes

$$Dst(T) = \frac{\sum_{i=1}^{4}\Delta H_i}{\sum_{i=1}^{4}\cos\theta_i} \tag{2}$$

Using the four stations given here, the differences in the results are small. Furthermore, the formulation given by (1) allows us to intercompare the variations measured at each station.

[12] To determine the true disturbance field at individual stations we need a method to separate the long-term secular variation and the short-term solar daily variation, *Sq*, from the magnetic recordings. Here we will basically follow the same statistical procedure as is used in the computation of the official *Dst* index [*Sugiura and Kamei*, 1991].

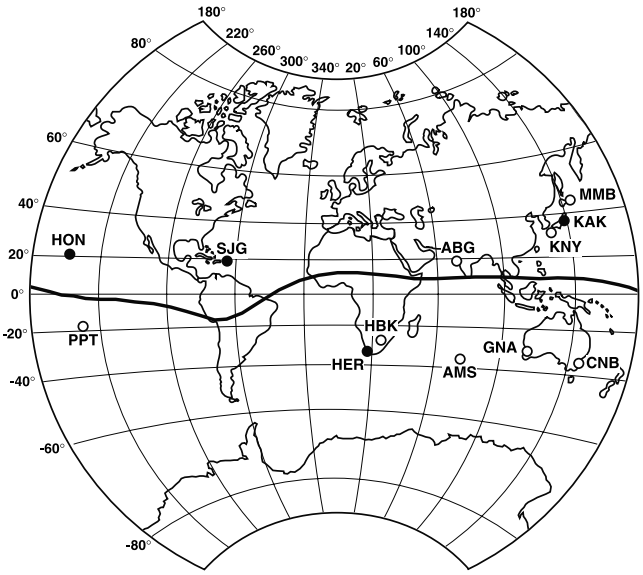

Figure 1. Locations of several geomagnetic observatories. The solid circles mark the official *Dst* stations KAK, HER, HON, and SJG. The open circles show the locations of other stations used in this study. The solid line marks the magnetic dip equator.

[13] In removing the secular variation, we first compute for each year an annual average of the horizontal component H. This annual average is computed from the five internationally quietest days of each month. Then for each year we take the annual average of that year and four previous years and fit a second-order polynomial to these points. To minimize the possible effects of discontinuities in the fittings between successive years an additional step is made. From the polynomial expansion determined in the first step, the baseline value at the end of the current year is calculated. This value is then included as an additional data point in a new second-order polynomial fitting. Using this fit, we are then able to evaluate the baseline, $H_0(T)$, for any day of the year.

[14] To subtract the solar quiet daily variation, *Sq*, from the data we need to determine the *Sq* curves for each day separately. The official method uses statistical analysis where *Sq* is expanded as a double Fourier series in local time (LT) T and month number M

$$Sq(T,M) = \sum_{m=1}^{6}\sum_{n=1}^{6} A_{mn} cos(mT + \alpha_m) cos(nM + \beta_n) \qquad (3)$$

The series contains 48 unknown coefficients A_{mn}, α_m, and β_n. These are determined by computing one *Sq* curve for each month as an average of the variation curves of the five quietest days of the month. A possible linear trend from a local midnight to the following local midnight in these *Sq* variations is subtracted. These *Sq* curves give us 288 data points so the coefficients may be determined by usual least squares fitting methods. Once the coefficients are known, the *Sq* variation may be computed for any day and any hour of the year. It should be emphasized that this method of *Sq* removal is statistical by nature and will not reproduce very accurately the *Sq* for any single day. However, the statistical method is probably the most suitable since the true *Sq* curve cannot be identified with sufficient accuracy for every day.

[15] The disturbance field $\Delta H(T)$ used for the *Dst* determination is then finally

$$\Delta H(T) = H(T) - H_0(T) - Sq(T,M) \qquad (4)$$

2.2. Two Methods for Subtracting the Secular Variation

[16] In determining the annual averages from the quiet day curves an important question is how the daily averages are computed. The averages can be computed as whole day (24-hour) averages or alternatively the local midnight levels can be used as the baseline.

[17] It is clear that these two methods lead to different baseline values as the whole day average values depend on the shape of the *Sq* curve. As the shape of the *Sq* curve changes from month to month, the difference in baselines between these two methods does not remain constant. Furthermore, the *Sq* curves for different stations are very different which leads to consistent offsets in measured disturbance values at different stations between these two computation methods. This is especially clearly seen at HON and SJG (see section 3) where the whole day averaging method leads to higher measured disturbance values. In

Table 1. Geomagnetic Observatories, Their Acronyms, Geographic and Geomagnetic Locations (in Degrees), and Periods When Data From These Stations are Available

Station Name	Acronym	Geographic Latitude	Geographic Longitude	Geomagnetic Latitude	Geomagnetic Longitude	Data Coverage
San Juan	SJG	18.4	293.9	29.4	5.2	1950–1999
Honolulu	HON	21.3	202.0	21.5	268.6	1950–1999
Kakioka	KAK	36.2	140.2	26.6	207.8	1950–1999
Hermanus	HER	−34.4	19.2	−33.7	82.7	1950–1999
Memambetsu	MMB	43.9	144.2	34.6	210.2	1957–1999
Alibag	ABG	18.6	72.9	9.6	145.4	1950–1999
Martin de Vivies	AMS	−37.8	77.6	−46.9	142.8	1981–1999
Canberra	CNB	−35.3	149.4	−43.4	226.1	1979–1999
Gnangara	GNA	−31.8	115.9	−42.7	187.9	1957–1999
Kanoya	KNY	31.4	130.9	21.1	199.9	1958–1999
Papeete	PPT	−17.6	210.4	−15.1	284.4	1968–1999
Hartebeesthoek	HBK	−25.9	27.7	−27.0	93.1	1971–1999

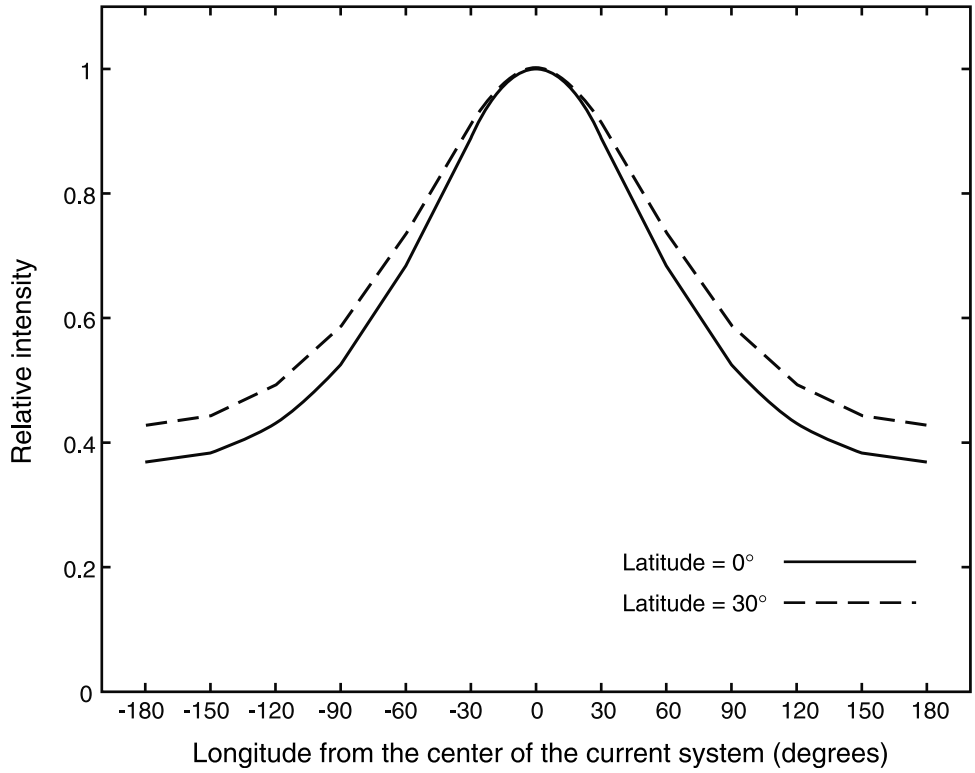

Figure 2. Relative intensities of the *H* component as measured at Earth's equator and at latitude 30° caused by a 30° wide partial ring current system at a distance of 4 R_E. The horizontal axis gives the difference in longitude from the point under the center of the current system.

the following analysis, we use midnight levels as daily averages when computing the secular variation. To distinguish our results from the official *Dst* method (24-hour averages), we call this the "base method" for baseline subtraction.

2.3. *Dst* Computation From Individual Station Data

[18] It is well established that the strongest magnetic variations, geomagnetic storms, are associated with the formation of a strongly asymmetric ring current, which maximizes in the evening sector. The asymmetry is especially pronounced during the storm main phase, and becomes smaller during the storm recovery phase. Thus, near storm maximum the four stations at different magnetic LTs will record a different disturbance depending on how far they are from the partial ring current system. Furthermore, the partial ring current is also closed via the ionosphere, which leads to stronger observed disturbances at longitudes where the field-aligned currents are strong. As the field-aligned currents cause both *D* and *H* variations, their contribution can be analyzed by examining the *D* component variations.

[19] To get a first-order estimate of the intensity variations at the four stations, we assume a portion of the partial ring current (not closed to the ionosphere) that has an angular width of 30° at a distance of 4 R_E. Figure 2 shows the relative intensities of the *H* component disturbance measured at the equator at different longitudes from the center of the current system. Note that there is about 60% attenuation of the signal on the other side of the Earth. This represents a lower limit of the true attenuation, as neither effects of conducting Earth between the current and the point of observation nor effects of the current closure to the ionosphere were included in the computation. This demonstrates the importance of an even station coverage.

[20] Figure 3a shows the differences between the official *Dst* obtained from the World Data Center and the *Dst* index computed from the individual station data using 24-hour daily averages color coded as functions of DOY and UT. The data have been averaged over the time period 1957–1999 when data from all four stations were available, and are shown in 14-day by 1-hour bins. Note that the differences are quite consistently about 3 nT, without any recognizable structure in the plot. This indicates that data from the individual stations are treated systematically similarly to the official *Dst* index computation. The reason for the 3 nT difference is not clear, but it is most probably an effect of the long-term baseline and secular variation subtraction. However, the smallness and uniformity of the error means that our computed *Dst* can be used to analyze the effects that are present in the official *Dst* index.

[21] Figure 3b shows, in a similar format to Figure 3a, the difference between the official *Dst* and the *Dst* computed using the "base method" for the secular variation subtraction. Note that now there is a consistent increase in the errors at equinoxes, which arises from the different computation of the baselines at the individual stations. Note also that because *Dst* is computed as an average over the stations, the different baselines at the four stations do not cause any additional diurnal variation in the index.

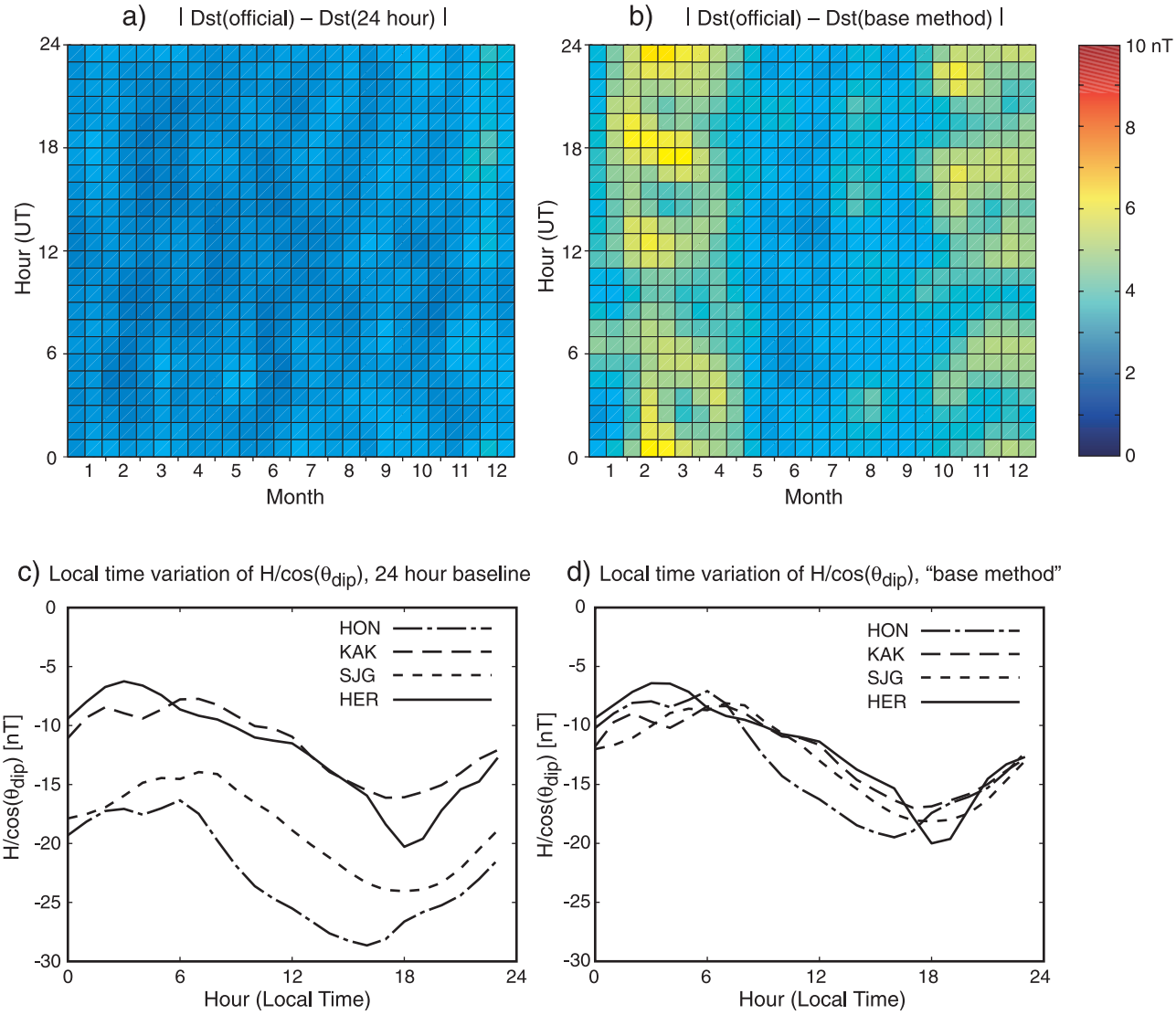

Figure 3. (a) *Dst*(official) − *Dst*(computed) using the official baseline subtraction method color coded as a function of DOY and UT. (b) *Dst*(official) − *Dst*(computed) using the "base method" (see text for details) color coded as a function of DOY and UT. (c) LT variation of $\Delta H/\cos\theta$ for the *Dst* stations using the 24-hour baseline subtraction method. (d) LT variation of $\Delta H/\cos\theta$ for the *Dst* stations using the "base method" for secular variation subtraction.

[22] Figures 3c and 3d show the average daily variation of the horizontal field at the four *Dst* observatories, now averaged over all days of year and all available years, using the official secular variation subtraction method and the "base method," respectively. Plotting the variations as a function of LT rather than UT shows that there is a consistent LT variation at the stations used to compute the *Dst* index, with maximum activity near 18 LT and minimum activity near 06 LT. This is quite naturally explained by the formation of a strong partial ring current in the midnight–evening sector, and the loss of current-carrying particles in the dayside. Note also that there is a consistent offset in the activity levels for SJG and HON when the official secular variation subtraction method is used (Figure 3c): the LT curves from SJG and HON are about 10 nT below HER and KAK. This offset is corrected when the "base method" is used (Figure 3d).

[23] Correction of the long-term baselines to the same levels at all stations results in increased errors when comparing our computed *Dst* using the "base method" and the official *Dst* index (Figure 3b). This indicates that some of the variability found in the *Dst* index may actually be caused simply by the different baselines in the individual station data. The magnitude of this effect is examined in more detail in the following sections.

3. Selection of *Dst* Stations

3.1. Stations for the Official *Dst* Index

[24] The previous section and Figure 3 show clear evidence that in order to compare the disturbance amplitudes between stations it is important to correct for the baselines such that the average variations are similar at each station. Therefore, in all subsequent analyses, the "base method" is

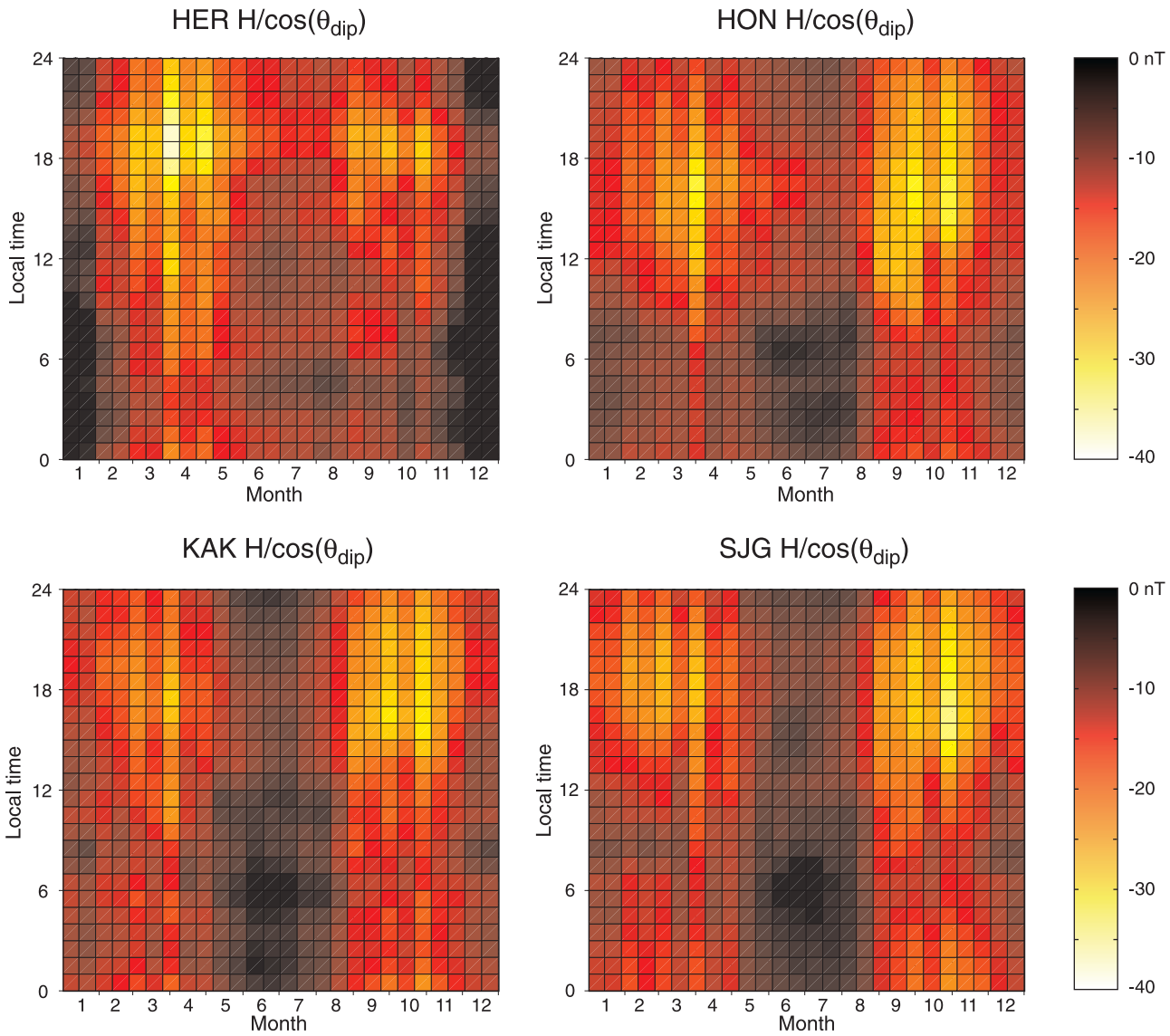

Figure 4. $\Delta H/\cos\theta$ for the four *Dst* stations KAK, HON, SJG, and HER using the "base method" for secular variation subtraction. The data are shown color coded as functions of DOY and LT.

utilized for the secular variation subtraction. This gives similar baselines for all magnetic stations used in this study.

[25] In this section, we examine the averaged field variations at the four *Dst* stations. For easier comparison of data from different stations, we plot the quantities $\Delta H/\cos\theta$ as functions of LT (instead of UT) and DOY, averaged over the years 1950–1999 when data from all stations were available.

[26] Figure 4 shows $\Delta H/\cos\theta$ for each of the *Dst* stations in the format described above. Note that all stations show a maximum around 18 LT, which is due to the partial ring current maximum in that region when (stormtime) ring current particles are injected from the nightside magnetosphere. The maxima are strongest near the spring and fall equinoxes when the magnetic activity is most intense. Note that the fall maximum is stronger than the spring maximum at the Northern Hemisphere stations, whereas the spring maximum is stronger at HER in the Southern Hemisphere.

[27] Furthermore, there is also a clear difference in the summer and winter minima, such that the Northern Hemisphere stations show a deeper activity minimum in the summer months (June–August), while HER in the Southern Hemisphere shows an opposite behavior with a deeper minimum in the seasonal activity during the winter months (December–February).

3.2. Alternative Station Distribution: Dst_6

[28] As shown in Figure 4, there are clear seasonal differences between stations in opposite hemispheres. In order to get a more balanced index, we selected, in addition to the three Northern Hemisphere stations (KAK, HON, and SJG), three Southern Hemisphere stations HER, PPT, and GNA. This network of six stations provides a good longitude coverage over the globe, and an even distribution of stations between the Northern and Southern Hemispheres (Figure 5). The index created applying the normal method

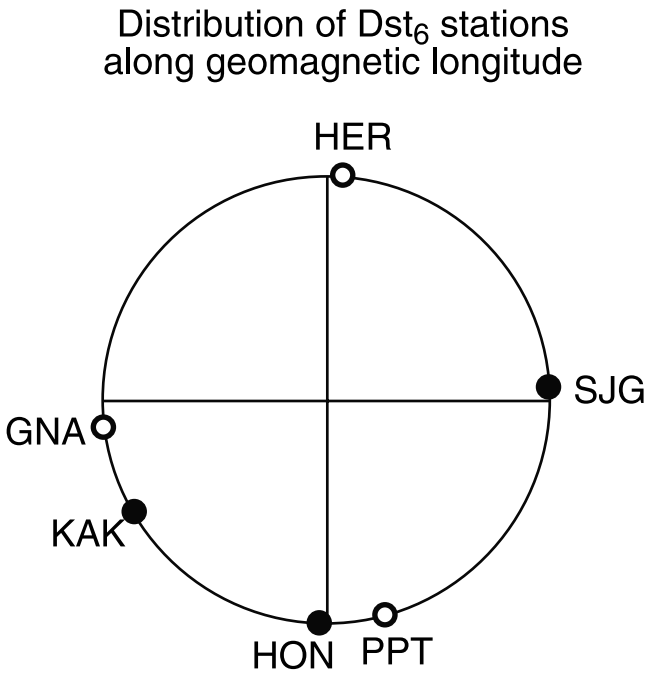

Figure 5. Longitudinal distribution of the selected stations for Dst_6. Northern Hemisphere stations are shown with filled circles and Southern Hemisphere stations with open circles.

of *Dst* computation but using data from these six stations is termed Dst_6.

[29] Ideally, one would like to use 8 stations, one in all longitudinal quadrants in both hemispheres. However, the European stations in the longitudinal sector of HER are all at relatively high latitudes (or data are not available over long time periods). It was therefore concluded that the noise signals caused by auroral electrojets would be more harmful than the lack of a Northern Hemisphere station in this longitudinal sector. On the other hand, in Latin America, in the longitudinal sector of SJG, there were no long time series from suitably located stations available in digital form. Therefore, the Dst_6 is a compromise representing an improvement but not an ideal solution to the index computation.

[30] Figure 6a shows the yearly variation, averaged over LTs, separately for several Northern and Southern Hemisphere stations (see Table 1 for station locations). The averages have been computed for the periods when data from all of these stations were available. This plot shows marked differences between the two hemispheres. While in the Northern Hemisphere the summer activity minimum and fall activity maximum are about 5 nT larger than the winter minimum and spring maximum, in the Southern Hemisphere the opposite is true but with a larger amplitude. The behavior is very similar at all stations.

[31] The antisymmetry is further illustrated in Figure 6b, where the Northern and Southern Hemisphere observations are shown as functions of local season. The curves show very similar behavior with lower activity (less negative values) in local spring and summer, and higher activity during fall and winter. The amplitude difference between Northern and Southern Hemispheres is quite consistent and therefore not dependent on the choice of the individual

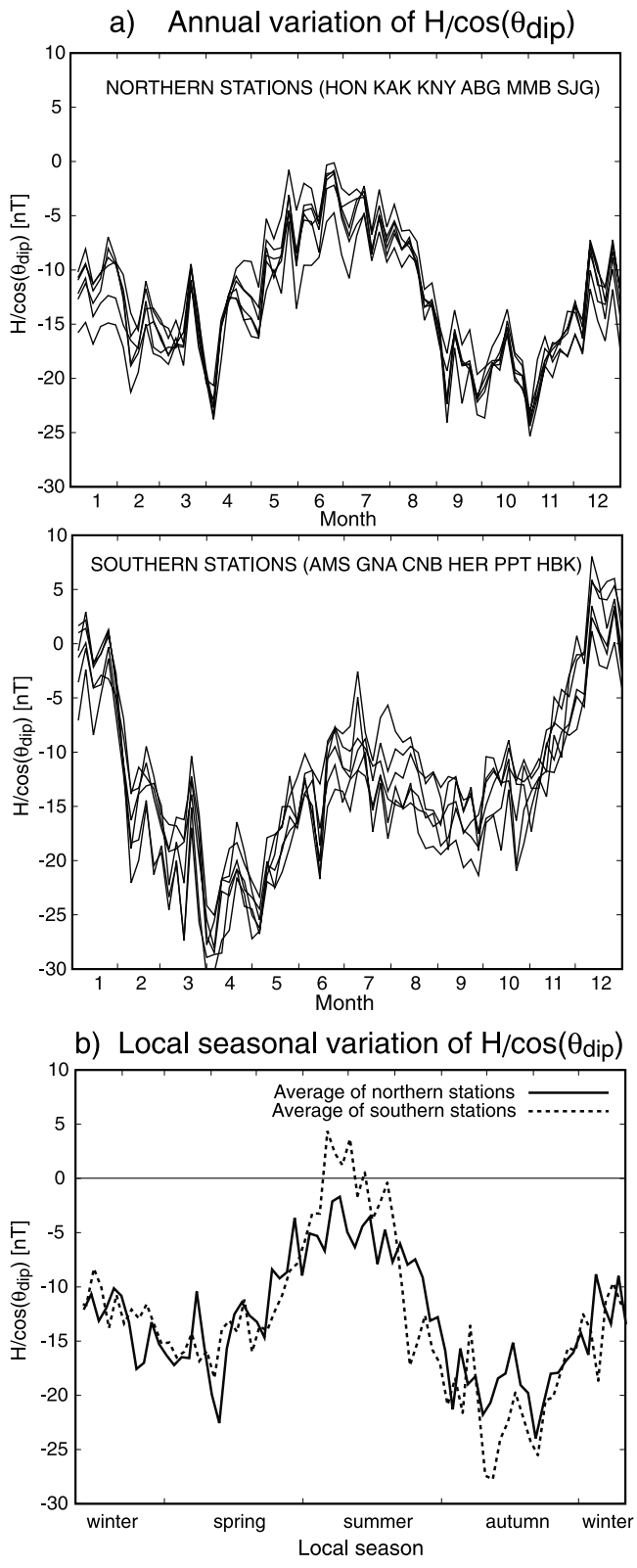

Figure 6. (a) Annual variation of $\Delta H/\cos\theta$ at the Northern Hemisphere stations KAK, HON, SJG, KNY, MMB, and ABG (upper panel) and at the Southern Hemisphere stations HER, HBK, AMS, GNA, CNB, and PPT (lower panel) using the "base method" for secular variation subtraction. (b) Local seasonal variation of $\Delta H/\cos\theta$ averaged over the six northern stations (solid line) and over the six southern stations (dashed line).

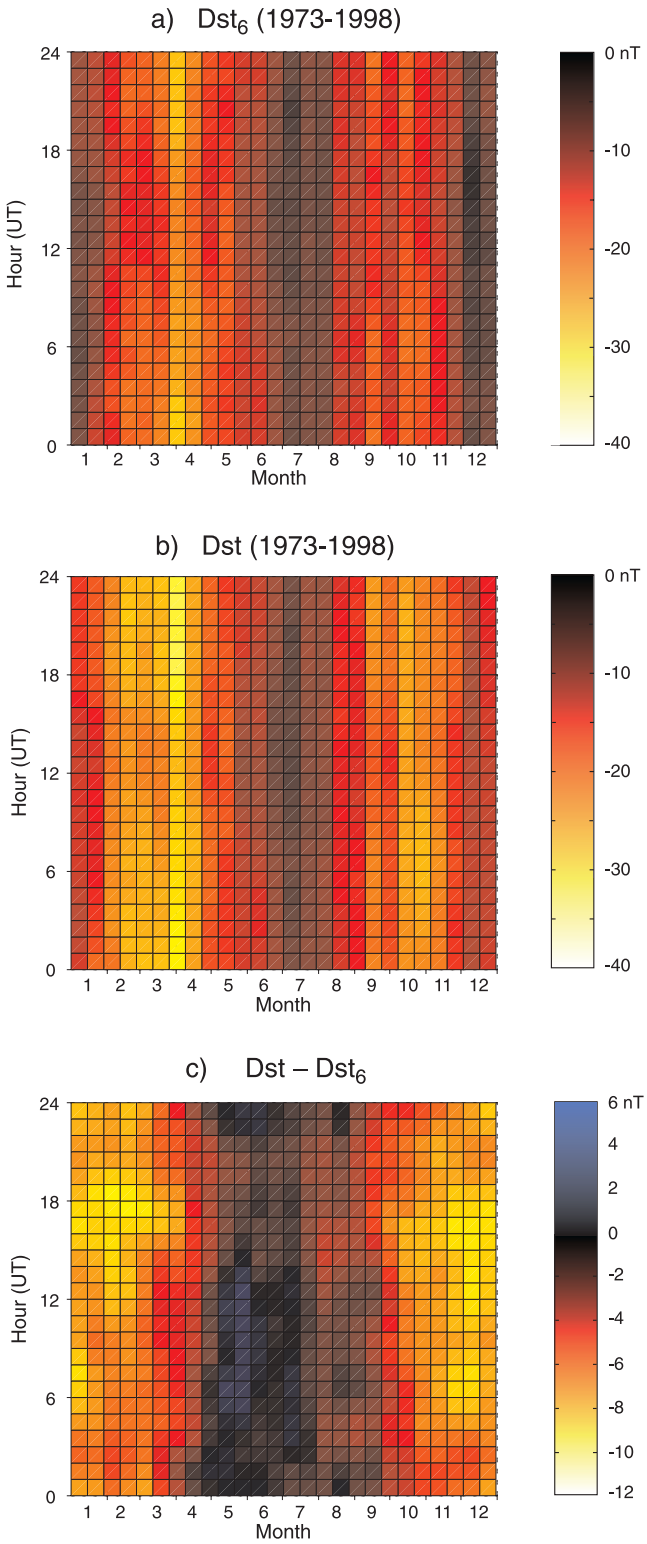

Figure 7. (a) Dst_6 color coded as function of DOY and UT. (b) Official *Dst* (time limited to periods when Dst_6 could be computed) color coded as function of DOY and UT. (c) $Dst - Dst_6$ color coded as function of DOY and UT.

stations, but may be affected by the asymmetric structure of the main field. From these results, it is clear that it is important to include both Southern and Northern Hemisphere stations with equal weights when the seasonal and diurnal variations of geomagnetic activity are evaluated. The causes for the seasonal, diurnal, and hemispheric differences are discussed in detail below.

3.3. Annual and Diurnal Variability in Dst_6

[32] Figure 7 shows a LT–DOY map for the Dst_6 and *Dst* indices and their difference computed using the data from 1973 to 1999 (both indices are computed from a data set covering the same time period). As compared to the *Dst* computed from the full data set, the official *Dst* becomes less smooth as the number of data points is reduced, but the basic features remain the same.

[33] It is clear that in the Dst_6 index the summer–winter difference is much smaller than in the official *Dst* index, which shows a clear annual minimum during northern summer. Similarly, the spring and fall maxima are more equal in intensity in Dst_6, while the official *Dst* shows a much stronger spring maximum than the fall maximum. Note also that Dst_6 shows a slightly lower average level of activity, which is probably due to the additional stations, which reduce the weight of the station recording the maximum disturbance.

[34] The difference map between *Dst* and Dst_6 (Figure 7c) shows a clear annual as well as diurnal pattern: The difference is mostly positive during the summer and maximizes in May and June around 9–12 UT; the error is almost zero but slightly negative around 18 UT. The error obtains the largest negative values near the equinoxes as well as during the winter months. The difference in the spring minimizes around 18 UT, in the fall there is a double minimum with peaks near 18 and 06 UT.

[35] The semiannual pattern in the difference matrix comes from the baseline corrections: The *Sq* curves, which are subtracted from the data, vary from month to month. As the used baselines are different for the official *Dst* and Dst_6, the annual pattern of the *Sq* curves is seen in the differences. Furthermore, the more even station distribution affects the annual variation: the equal number of Southern and Northern Hemisphere stations increases the activity during the summer activity minimum and, on the other hand, decreases activity during the winter minimum. Therefore, the differences are negative during fall, winter, and spring, but positive during the summer months.

[36] The diurnal variation shows a pattern where the annual variability is largest around 12 UT and 18 UT, where the differences are negative near equinoxes and positive or near zero during the summer solstice. On the other hand, around 00 and 06 UT there is much less annual variability in the differences with both the equinox minima and the summer maxima being smaller in amplitude. In the Dst_6 data, the spring equinox and summer solstice show smaller values at 00 and 06 UT than at 12 and 18 UT. This would indicate that adding two stations at longitudes which are at 18 LT at 00 and 06 UT (GNA and PPT, respectively) increases the spring and summer activity, which are dominated by the Southern Hemisphere stations.

4. Seasonal and Diurnal Variability in the External Driver

4.1. Three External Drivers of Geomagnetic Activity

[37] As discussed in the introduction, there are three geometrical factors which may contribute to the annual

and diurnal variability of the external driving. In order to examine the relative contributions of each of the three driver mechanisms, we define three matrices, which are associated with the three angles in the UT–DOY space, in 1-hour and 14-day averages similar to the data treatment.

1. Axial hypothesis: The heliographic latitude of the Earth λ obtains its extreme values on 7 September (Northern Hemisphere) and on 6 March (Southern Hemisphere), thus being close to zero near solstices. The heliographic latitude has no UT dependence and is therefore only a function of the DOY. The angle λ varies between $-7.25°$ and $+7.25°$.

2. Equinoctial hypothesis: The direction of the solar wind flow is roughly along the Sun–Earth line, and hence annual and UT patterns of the angle ϕ between the flow direction and the dipole field can be computed from the orientation of the dipole field. Computation of the angle ϕ requires knowledge of the direction of the Sun relative to the orientation of the dipole; the formulas can be found in the study of *Russell* [1971]. The value of ϕ ranges from 55° to 125°. The range of the acute angle between the Sun–Earth line and the dipole axis (ϕ_A) is 55°–90°. In careful analysis one should take the aberration effect into account [*Roosen*, 1966; *Mayaud*, 1974]. The aberration effect causes an apparent angular offset to the solar wind direction. This results in a shift of about 4 days (for average wind speed of 438 km/s) of the DOY–UT plot of the angle ϕ_A along the DOY axis in the positive direction.

3. Russell–McPherron effect: The angle ψ between the z axis in the GSM coordinate system and the solar equatorial plane governing the reconnection rate according to the Russell–McPherron hypothesis can also be computed from the direction of the Sun relative to geomagnetic coordinates. Coordinate transformation from GSEQ (geocentric solar equatorial coordinate system) to GSM coordinates can be found in the study of *Russell* [1971]. The Russell–McPherron angle ψ varies from 52° to 90°. Magnetic activity is expected to reach maximum levels when ψ is at minimum which occurs on 5 April and 5 October.

[38] Figure 8 shows contour plots of the three angles λ, ϕ_A (aberration corrected), and ψ. It is clear that each of the effects produces distinct UT and annual variability patterns, and hence their contribution should be identifiable from the data. Note that since all effects show semiannual variability with activity maxima near equinoxes, it is necessary to examine both the UT and DOY variations in order to distinguish between these effects.

4.2. Other Factors Affecting Dst_6

[39] In addition to the three effects described above there are other effects, both internal and external to the magnetosphere, which affect the magnetic recordings that are used to create Dst_6.

[40] Higher activity during the midwinter months than during midsummer months in the auroral regions has been associated with the lesser solar illumination of the polar ionospheres. This causes lower ionospheric conductivity, which in turn creates conditions more favorable for electron acceleration events [*Newell et al.*, 1996]. If the recordings are sensitive to strong electrojet currents during storm times, this could be a factor producing the higher activity during winter months at both hemispheres, and be one cause for the hemispheric asymmetry.

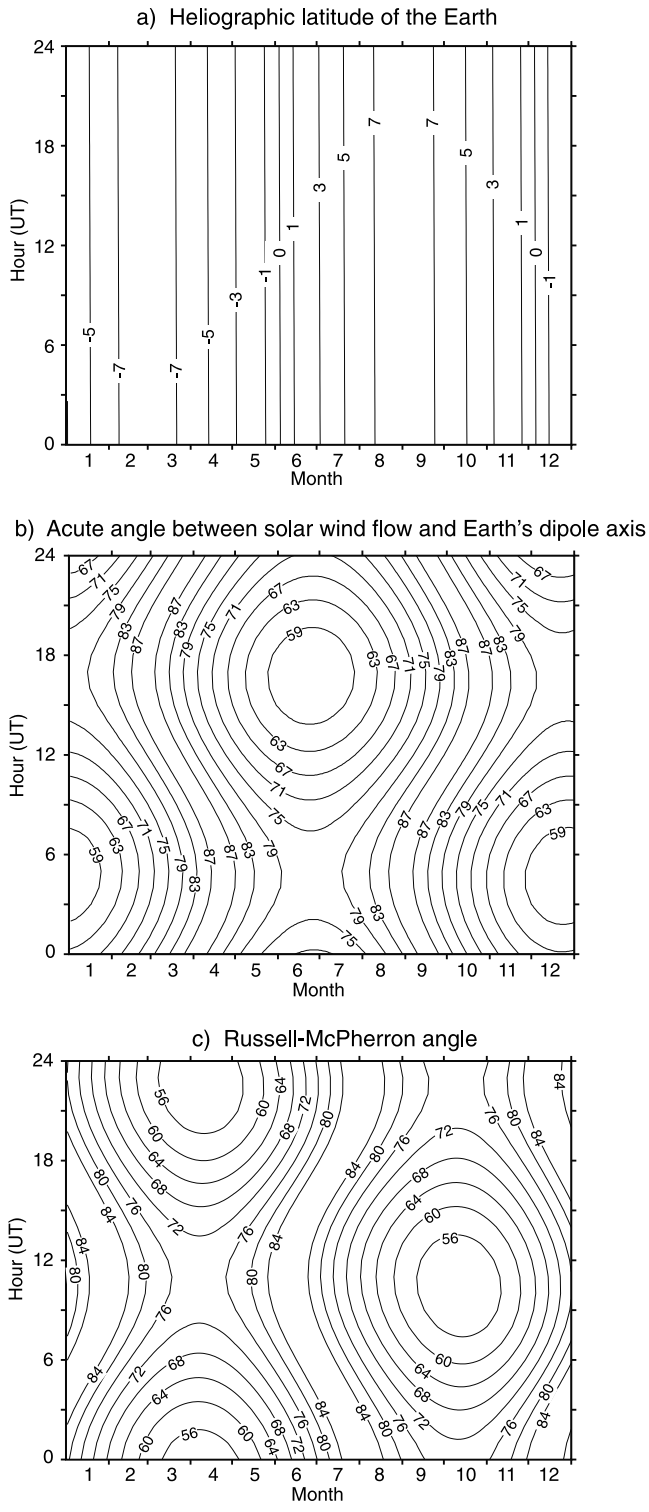

Figure 8. (a) Heliographic latitude of the Earth λ as function of DOY and UT. (b) Acute angle ϕ_A between the aberration corrected solar wind flow velocity and the Earth's magnetic dipole axis as function of DOY and UT. (c) Angle ψ between the z axis in the GSM coordinate system and the solar equatorial plane (Russell–McPherron angle) as function of DOY and UT.

[41] In northern winter, the dipole tilt axis is tilted antisunward. As the magnetotail orientation is along the Sun–Earth line (dictated by the solar wind flow velocity direction) the ring current, which is roughly at the geomagnetic equator, is bended northward near its outer edge as a consequence of the interaction between the magnetotail and inner magnetosphere current systems. Therefore, the activity at midnight is slightly closer to Northern Hemisphere stations than Southern Hemisphere stations at the same latitude, and hence the Northern Hemisphere activity is higher during northern winter. Similarly, the Southern Hemisphere activity is higher during southern winter.

[42] As the Sun rotates around its axis, different parts of its tilted magnetic field sweep past the Earth, creating a sector structure in the IMF. In a tilted dipolar field, two sectors, "away" from the Sun, and "toward" the Sun are observed. As the Earth's axis is tilted toward the direction of motion along its trajectory during the fall equinox, the maximum activity is associated with the toward polarity of the IMF, which provides maximally antiparallel IMF fields with the geomagnetic dipole field. Similarly, during the spring, maximum activity is associated with the away polarity of the IMF [*Berthelier*, 1976; *Oksman and Kataja*, 1986; *Silverman*, 1986]. As the sector structure is dependent on solar rotations rather than Earth's orbital characteristics, this effect should be rather randomly distributed over time, and should thus not cause asymmetries in the observed activity.

[43] The asymmetry in the main field is such that the field minimizes in the Southern Hemisphere, at the South Atlantic anomaly. This field asymmetry may cause N-S amplitude differences, which would not show a specific annual pattern, but would be randomly distributed over time.

4.3. Fitting External Driver Properties to Dst_6

[44] Assuming that the three effects driving geomagnetic activity explained in section 4.1. act in independent ways, the Dst_6 index can be modeled as a linear combination of these three effects:

$$Dst_{EXT} = A\Lambda + B\Phi + C\Psi + D \tag{5}$$

where Dst_{EXT} is the part of *Dst* driven by the three driver mechanisms. Λ, Φ, and Ψ are matrices defining the contributions to the *Dst* index based on the annual and diurnal variability of the angles λ, ϕ_A, and ψ in the UT–DOY space in 1-hour and 14-day averages, and A, B, C, and D are constants. Since each of the matrices has its own characteristic UT–DOY dependence, the relative magnitudes of the effects can be determined by minimizing the difference matrix $Dst_6 - Dst_{EXT}$ with respect to the constants A, B, C, and D. In this representation, the function to be minimized can be given as a standard error function

$$\sigma = \sum_{\mathrm{DOY}} \sum_{\mathrm{UT}} (Dst_6 - Dst_{EXT})^2 \tag{6}$$

where the summation over UT is from 0 to 23 with steps of 1 hour, and the summation over days of year is from 1 to 364 with steps of 14 days.

[45] The form of the matrices Λ, Φ, and Ψ may be freely chosen. Since we are dealing with angles, it is natural to choose forms with trigonometric functions. Furthermore, we normalize the functions between -1 and 0 so that the constants A, B, and C directly give the amplitudes of the three different effects. For these reason, we have chosen the functions $\Lambda = -\sin(|\lambda|)/\sin(\lambda_{max})$, $\Phi = -\sin(\phi_A - \phi_{A,min})/\sin(90^\circ - \phi_{A,min})$, and $\Psi = -\cos(\psi)/\cos(\psi_{min})$, where $\lambda_{max} = 7.3^\circ$, $\phi_{A,min} = 55^\circ$ and $\psi_{min} = 52^\circ$. With these selections, the values of the functions vary between 0 and -1, the function reaching the value -1 when the effect leads to highest magnetic activity (*Dst* most negative). However, the minimizing procedure does not seem to be very sensitive to the functional form used. We also tried squares of trigonometric functions and absolute values of the angles themselves as well as various products of trigonometric functions, but the results discussed in more detail below remained basically the same.

4.4. Results From Fitting Procedure

[46] Figure 9a shows the results from the fitting Dst_{EXT} to Dst_6 as described above. The fitting parameters obtained were $A = 3.3$ nT, $B = 5.9$ nT, $C = 9.4$ nT, and $D = -2.6$ nT, where the first three coefficients give the relative importance of the heliographic latitude, the equinoctial effect, and the Russell–McPherron effect, respectively. Thus, this result would suggest that of the three external driver mechanisms the Russell–McPherron effect is slightly above 50% in Dst_{EXT}, the equinoctial effect about 30%, and the heliographic latitude effect about 20%.

[47] Comparison of Figure 9a with the original Dst_6 in Figure 7a shows, however, that the fit is far from perfect. The correlation coefficient r^2 (= "explained variation/total variation") is 0.50 for this fit. Figure 9b shows the difference between Dst_6 and Dst_{EXT}, which reveals a clear annual and diurnal pattern. This indicates that there are other effects influencing the seasonal and diurnal variability of geomagnetic activity, which are not included in the three drivers described above. Roughly, the three drivers can account for about half of the observed *Dst* variability whereas the other half is caused by other sources. Furthermore, due to the poor fit, the evaluation of the relative importance of the three driver effects may not be accurate to high precision.

[48] Performing a similar fit of Dst_{EXT} to original *Dst* gives coefficients $A = 3.4$ nT, $B = 5.0$ nT, $C = 8.1$ nT, and $D = -7.4$ nT with $r^2 = 0.47$. If we compare these results to those of Dst_6 we note that the relative contribution of different effects remain practically unchanged. This result implies that the longitudinal asymmetry of Dst_6 is not the reason for the apparent dominance of the Russell–McPherron effect.

[49] Figure 9c shows Dst_6 for only periods when the activity was low and the index was above the level of -20 nT. When the fitting is performed again now to only data during quiet intervals, the fit is slightly better with $r^2 = 0.53$. The differences plotted in Figure 9d show that the errors are more than 50% lower than for the entire index, and the error matrix no longer shows clear diurnal or seasonal patterns. The obtained coefficients were $A = 1.5$ nT, $B = 1.6$ nT, $C = 2.1$ nT, and $D = 0.2$ nT, giving very similar relative magnitudes of the effects as for the full data set, again showing the Russell–McPherron effect as the dominant one. If a similar analysis is performed to only high-activity periods ($Dst_6 \leq -20$ nT), the coefficients are $A = 0.1$ nT,

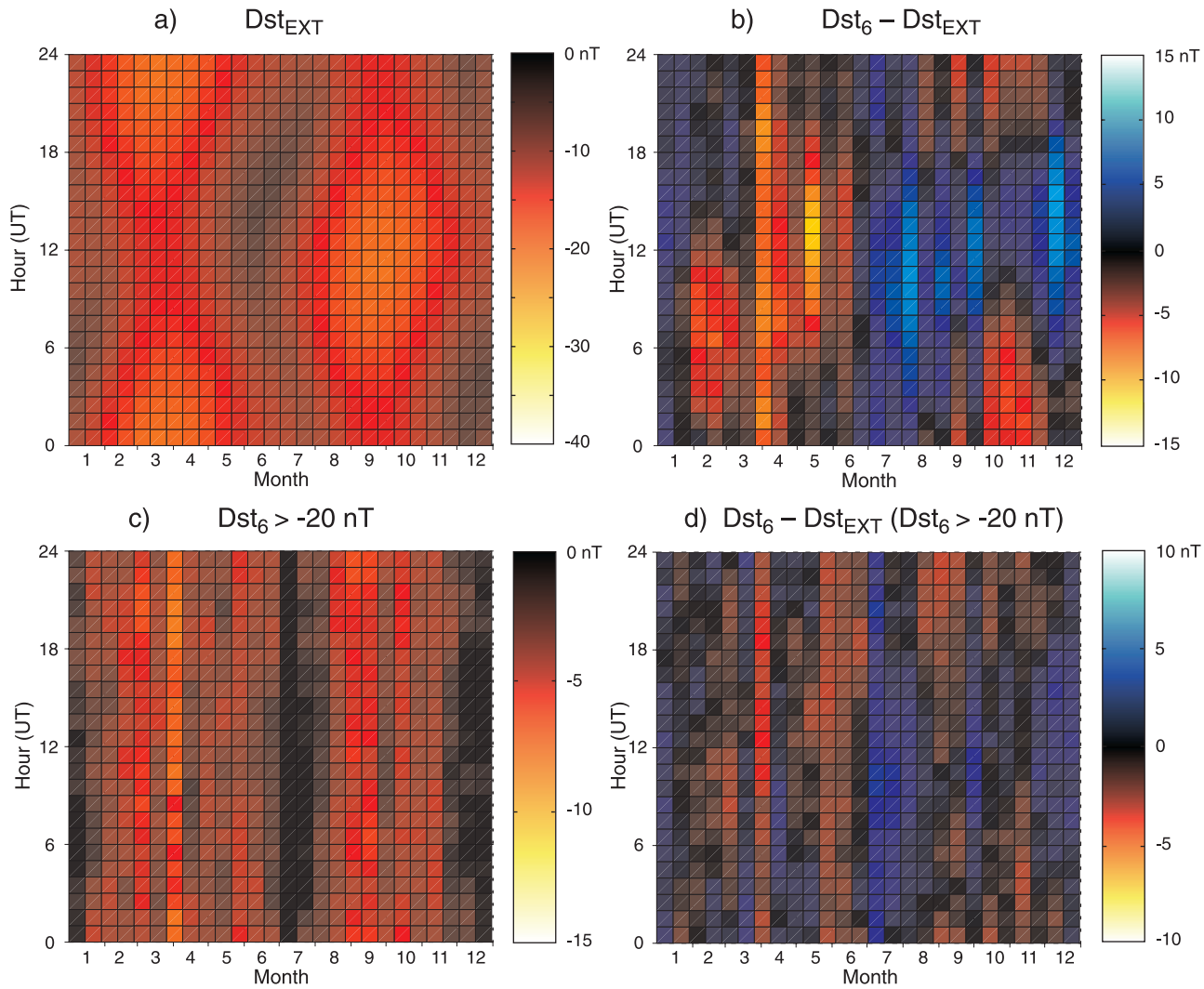

Figure 9. (a) Dst_{EXT} color coded as function of DOY and UT. (b) $Dst_6 - Dst_{EXT}$. (c) Dst_6 for low-activity periods ($Dst_6 > -20$ nT). (d) $Dst_6 - Dst_{EXT}$ for low-activity periods ($Dst_6 > -20$ nT).

$B = 3.0$ nT, $C = 3.9$ nT, and $D = -34.4$ nT, emphasizing the role of the Russell–McPherron effect during storm and other increased-activity periods. However, the fit is very poor with $r^2 = 0.21$.

5. Discussion and Conclusions

[50] In this paper we have examined data from stations used to create the official *Dst* index as well as from several other stations at equivalent locations. Long time series of these data were studied as functions of LT and season. The results revealed a significant diurnal variation in the level of disturbance such that the strongest variations are observed for all stations near 18 LT and the weakest variations near 06 LT, which is consistent with the partial ring current particles contributing in the midnight–evening sector, and these particles being lost from the inner magnetosphere either to the dayside magnetopause or to the ionosphere near local noon [*Ebihara and Ejiri*, 2000].

[51] Examination of individual station data also revealed that using the official method for subtracting the secular variations, different stations had substantially (about 10 nT) different average levels of activity, even though the diurnal and annual variations and their amplitudes were similar from station to station. This led us to introduce a "base method" for the elimination of the secular variation, which corrects for these differences such that the baselines are similar at all stations. The differences in baselines introduce a seasonal variation in the *Dst* index, whose magnitude is of the order of 3 nT (see Figures 3b and 9c).

[52] The individual station data also revealed a strong hemispheric dependence on the annual variation. In the Northern Hemisphere, the activity minimum was found during the summer solstice, the winter solstice showing about 10 nT stronger level of disturbance. The activity maximum was found during the fall equinox, the spring maximum being about 5 nT weaker than the fall maximum. On the other hand, in the Southern Hemisphere, the activity minimum was reached during the midwinter months, the summer minimum showing again about 10 nT stronger disturbances. The activity maximum occurs close to the spring equinox, and it is about 10 nT stronger than the fall maximum. The result that the difference between local fall and spring maxima is larger for the Southern Hemisphere

(Figure 6b) is consistent for all stations considered in this paper (and several other stations that were also examined but for which data are not shown), but its reason remains unclear. One possible explanation could be the asymmetry of the main field, which gives smaller average field in the Southern Hemisphere. This may be reflected in the magnetic records due to the different precipitation patterns.

[53] Differences in the auroral activity level between summer and winter have been recorded using both precipitating particle data [*Newell et al.*, 1996] and geomagnetic indices [*Ahn et al.*, 2000]. In the case of auroral activity, the large difference between the ionospheric conductance during local winter and summer is an obvious explanation: during the summer, the high conductivity prohibits the formation of large parallel potential drops, which reduces the number of electron acceleration events in the illuminated hemisphere [*Newell et al.*, 1996]. Furthermore, *Lyatsky et al.* [2001] argue that the activity maximizes during equinoxes when the nightside auroral zones of both hemispheres are in darkness.

[54] The official *Dst* index is computed from three Northern Hemisphere stations and one Southern Hemisphere station, which tends to overemphasize winter minimum and fall maximum levels of disturbances by several nT on the average. This led us to introduce a new index, Dst_6, which includes 6 stations, three from the northern and three from the Southern Hemisphere, with as equal LT coverage as possible. This index was created using the ''base method'' for baseline computation. These improvements should make Dst_6 better suited than *Dst* for examination of the causes of the diurnal and annual variability found in geomagnetic records.

[55] The seasonal and diurnal variation of Dst_6 is in the large scale similar to that of the official *Dst* [*Cliver et al.*, 2000]. However, there are several distinctions, which arise from the baseline changes as well as from the addition of two Southern Hemisphere stations: First, the summer and winter minima are now roughly of equal magnitude, which is a direct effect of having an equal number of Northern Hemisphere and Southern Hemisphere stations. Furthermore, the diurnal variation in Dst_6 is even weaker than in *Dst*, even though the diurnal effects are not very strongly present in *Dst* either. Note that neither of the indices shows clear characteristics of either the equinoctial or the Russell–McPherron effect [see also *Cliver et al.*, 2000].

[56] Different drivers of geomagnetic activity have been studied previously using both the *Dst* index [e.g., *Burton et al.*, 1975] and higher-latitude electrojet indices [*Cliver et al.*, 2000]. In this study, we conclude that only about half of the observed daily and seasonal variability can be accounted for by the three most well-known driver effects, the heliographic latitude, the equinoctial effect, and the Russell–McPherron effect. Of these three, the Russell–McPherron effect is clearly dominant giving about 50% contribution, and the heliographic latitude is least significant with about 20% contribution. *Cliver et al.* [2000] conclude that the Russell–McPherron effect accounts for only about 20% of the *am* index. They also conclude that the *Dst* index does not have a UT–DOY pattern that would resemble either the equinoctial or the Russell–McPherron effect patterns, but that the derivative of *Dst* giving the rate of change of the ring current intensity shows a clear pattern resembling that of the equinoctial effect. On the other hand, our results indicate that during magnetic storms, the Russell–McPherron effect is more dominant than the equinoctial effect if all levels of activity are considered. The reason for the discrepancy between these two results is not clear.

[57] *Akasofu* [1981] formulated the relationship between rate of energy input and *Dst* in the form

$$Q = -4 \times 10^{13} \left(\frac{dDst}{dt} + \frac{Dst}{\tau} \right) \tag{7}$$

where τ is the ring current decay rate in seconds. This would indicate that the rate of energy input is more directly tied to the derivative of *Dst* rather than the index itself. However, the second term in the equation depends on the loss rate, which is expressed through the exponential decay time τ. There are several studies examining the value of τ, which all conclude that the value of τ depends on geomagnetic activity, values range from as short as 1–2 hours during strong activity to 10–20 hours during magnetically quiet periods. For example, *O'Brien and McPherron* [2000] argue that τ in fact is also a function of the solar wind input in an exponential way. Therefore, the driving activity, value of *Dst*, and the derivative of *Dst* are tied together in a highly nonlinear fashion. This is readily seen by considering a period of northward IMF during a magnetically quiet period and during a storm recovery phase: in the first case the *Dst* derivative is zero while in the latter case the derivative is positive. Thus, neither the *Dst* index nor its derivative is free from the time history effects. Furthermore, as shown in this paper, the baseline subtraction method induces also daily variability, which would bring its effects also to the hour-to-hour variability of the index.

[58] Examining the diurnal variation only, *Takalo and Mursula* [2001] show that the activity maximizes at 12 UT and minimizes at 22 UT with a secondary minimum at 06 UT. They argue that the noon minimum is an effect that rises only from the lack of stations near 18 LT and because at the same time both HON and SJG stations show their daily maximum value. Their model of the *Dst* variation assumes a LT dependence of the geomagnetic activity that maximizes near 18 LT, and results in two minima near 06 and 20 UT and a maximum near 12 UT. This two-maximum pattern is also present in the Dst_6 index, and could be one of the contributing factors to the remaining half of the variability. However, the diurnal pattern should be slightly different using six stations instead of four, thus the pattern might be less pronounced for the case of Dst_6.

[59] The driver analysis performed here assumes that the factors contributing to the geomagnetic activity are randomly distributed both in UT and in season: if the IMF would have structure that would affect the N-S component in ways other than that dictated by the magnetospheric geometry (Russell–McPherron angle), this would of course give its imprints to the annual pattern. Similarly, the solar wind velocity or pressure could in principle affect the pattern through structuring in the solar wind. However, such structures have not been found; the IMF and solar wind have their periodicities related to solar activity, which do not coincide with the Earth's rotation periods. Therefore, the evaluation of the activity data (*Dst*) in terms of the purely geometrical factors is justified.

[60] It is important to note that the analysis performed here concerns the seasonal and diurnal variability of the *Dst* index over all periods of time, which means that it mostly reports on drivers during nonstorm times. Therefore, it is not unexpected that the results are not as clear as when individual storms are analyzed. We emphasize that the drivers of the *Dst* index over all time periods can show features that differ from the drivers of individual storms.

[61] In this paper, we have shown that the three external drivers as modeled by the three angles given by the heliographic latitude, the equinoctial hypothesis and the Russell–McPherron effect cannot account for more than about 50% of the observed daily and seasonal variability of the *Dst* index. With a simple model calculation we also showed that two stations 90° apart can measure up to 50% difference in intensity, if one of the stations is underneath the current system. As the signal intensity decreases strongly away from the current system, an ideal index with no diurnal effects from LT coverage would have to include stations with about 45° longitudinal separation, which would always result in recording at least 80% of the maximum intensity. Thus, assessment of the drivers of geomagnetic activity needs to carefully account for also these effects. Unfortunately, Dst_6 was the best station coverage that could be obtained by having a sufficiently large data set with enough data points in each individual bin of a UT–DOY matrix. This data set and our analysis suggest that the Russell–McPherron effect is the leading external driver, but that both the heliographic latitude and equinoctial effect are significant as well.

[62] **Acknowledgments.** We wish to thank both referees for their useful and constructive remarks.

References

Ahn, B.-H., H. W. Kroehl, Y. Kamide, and E. A. Kihn, Universal time variations of the auroral electrojet indices, *J. Geophys. Res.*, *105*, 267, 2000.

Akasofu, S.-I., Energy coupling between the solar wind and the magnetosphere, *Space Sci. Rev.*, *28*, 121, 1981.

Alexeev, I. I., E. S. Belenkaya, V. V. Kalegaev, Y. I. Feldstein, and A. Grafe, Magnetic storms and magnetotail currents, *J. Geophys. Res.*, *101*, 7737, 1996.

Bartels, J., Eine universelle Tagesperiode der erdmagnetischen Aktivität, *Meteorol. Z.*, *42*, 147, 1925.

Berthelier, A., Influence of the polarity of the interplanetary magnetic field on the annual and the diurnal variations of magnetic activity, *J. Geophys. Res.*, *81*, 4546, 1976.

Boller, B. R., and H. L. Stolov, Kelvin–Helmholtz instability and the semiannual variation of geomagnetic activity, *J. Geophys. Res.*, *75*, 6073, 1970.

Burton, R. K., R. L. McPherron, and C. T. Russell, An empirical relationship between interplanetary conditions and *Dst*, *J. Geophys. Res.*, *80*, 4204, 1975.

Cliver, E. W., Y. Kamide, and A. G. Ling, Mountains versus valleys: Semiannual variation of geomagnetic activity, *J. Geophys. Res.*, *105*, 2413, 2000.

Clua de Gonzalez, A., V. M. Silbergleit, W. D. Gonzalez, and B. T. Tsurutani, Annual variation of geomagnetic activity, *J. Atmos. Sol. Terr. Phys.*, *63*, 367, 2001.

Cortie, A. L., Sunspots and terrestrial magnetic phenomena, 1898–1911: The cause of the annual variation in magnetic disturbances, *Mon. Not. R. Astron. Soc.*, *73*, 52, 1912.

Currie, R. G., The geomagnetic spectrum: 40 days to 5.5 years, *J. Geophys. Res.*, *71*, 4579, 1966.

Ebihara, Y., and M. Ejiri, Simulation study of fundamental properties of the storm-time ring current, *J. Geophys. Res.*, *105*, 15,843, 2000.

Häkkinen, L. V. T., T. I. Pulkkinen, H. Nevanlinna, R. J. Pirjola, and E. I. Tanskanen, Effects of induced currents on *Dst* and on magnetic variations at mid-latitude stations, *J. Geophys. Res.*, *107*, SMP 7–1, 2002.

Jordanova, V. K., C. J. Farrugia, J. M. Quinn, R. M. Thorne, K. W. Ogilvie, R. P. Lepping, G. Lu, A. J. Lazarus, M. F. Thomsen, and R. D. Belian, Effect of wave–particle interactions on ring current evolution for January 10–11, 1997: Initial results, *Geophys. Res. Lett.*, *25*, 2971, 1998.

Lyatsky, W., P. T. Newell, and A. Hamza, Solar illumination as cause of the equinoctial preference for geomagnetic activity, *Geophys. Res. Lett.*, *28*, 2353, 2001.

Mayaud, P. N., Variation semi-annuelle de l'activité magnétique et vitesse du vent solaire, *C. R. Acad. Sci. Paris*, *278*, 139, 1974.

Mayaud, P. N., *Derivation, Meaning and Use of Geomagnetic Indices*, *Geophys. Monogr.*, vol. 22, pp. 1–154, AGU, Washington, D. C., 1980.

McIntosh, D. H., On the annual variation of magnetic disturbance, *Philos. Trans. R. Soc. London, Ser. A*, *251*, 525, 1959.

Menvielle, M., and A. Berthelier, The K-derived planetary indices: Description and availability, *Rev. Geophys.*, *29*, 415, 1991.

Newell, P. T., C.-I. Meng, and K. M. Lyons, Suppression of discrete aurorae by sunlight, *Nature*, *381*, 766, 1996.

O'Brien, P., and R. L. McPherron, An empirical phase space analysis of ring current dynamics: Solar wind control of injection and decay, *J. Geophys. Res.*, *105*, 7707, 2000.

Oksman, J., and E. Kataja, Hemispheric asymmetry of the sun suggested by the annual variation of the aa index, *Ann. Geophys.*, *4*, 69–74, 1986.

Pulkkinen, T. I., N. Yu. Ganushkina, D. N. Baker, N. E. Turner, J. F. Fennell, J. Roeder, T. A. Fritz, M. Grande, B. Kellett, and G. Kettmann, Ring current ion composition during solar minimum and rising solar activity: Polar/CAMMICE/MICS results, *J. Geophys. Res.*, *106*, 19,131, 2001.

Rangarajan, G. K., Indices of geomagnetic activity, in *Geomagnetism*, vol. 3, edited by J. A. Jacobs, pp. 323–384, Academic, San Diego, Calif., 1989.

Roosen, J., The seasonal variation of geomagnetic disturbance amplitudes, *Bull. Astron. Inst. Neth.*, *18*, 295, 1966.

Russell, C. T., Geophysical coordinate transformations, *Cosmic Electrodyn.*, *2*(2), 184, 1971.

Russell, C. T., and R. L. McPherron, Semiannual variation of geomagnetic activity, *J. Geophys. Res.*, *78*, 92, 1973.

Silverman, S. M., Annual variation of aurora and solar wind coupling, in *Solar Wind–Magnetosphere Coupling*, edited by Y. Kamide and J. A. Slavin, pp. 643–654, Terra Sci., Tokyo, 1986.

Sugiura, M., and T. Kamei, Equatorial *Dst* index 1957–1986, in *IAGA Bull.*, vol. 40, edited by A. Berthelier and M. Menvielle, pp. 1–246, ISGI Publ. Off., Saint Maur, 1991.

Takalo, J., and K. Mursula, A model for the diurnal variation of the *Dst* index, *J. Geophys. Res.*, *106*, 10,905, 2001.

Turner, N. E., D. N. Baker, T. I. Pulkkinen, and R. L. McPherron, Tail current contribution to *Dst*, *J. Geophys. Res.*, *105*, 5431, 2000.

Vennerstrom, S., and E. Friis-Christensen, Long-term and solar cycle variation of the ring-current, *J. Geophys. Res.*, *101*, 24,727, 1996.

L. V. T. Häkkinen, H. Nevanlinna, R. J. Pirjola, T. I. Pulkkinen, E. I. Tanskanen, and N. E. Turner, Geophysical Research, Finnish Meteorological Institute, P.O. Box 503, FIN-00101 Helsinki, Finland. (Lasse.Hakkinen@fmi.fi; Heikki.Nevanlinna@fmi.fi; Risto.Pirjola@fmi.fi; Tuija.Pulkkinen@fmi.fi; Eija.Tanskanen@fmi.fi; Niescja.Turner@fmi.fi)